

AD-A186 271

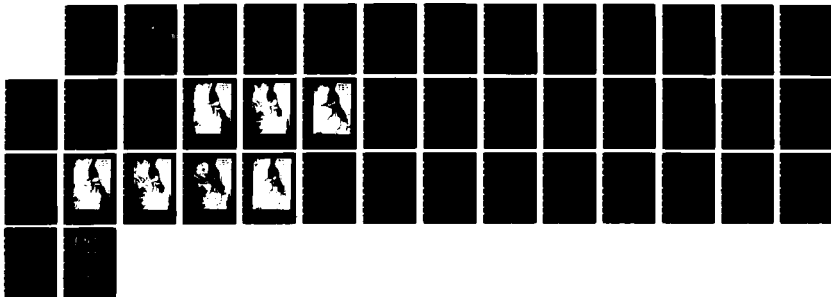
AN INVESTIGATION OF OFFSHORE CIRCULATION USING
SATELLITE DATA AND FEATURE TRACKING TECHNIQUES(U) NAVAL
POSTGRADUATE SCHOOL MONTEREY CA G R LENNON SEP 87

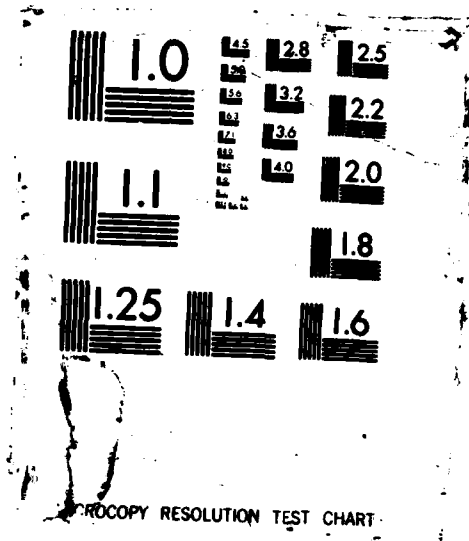
1/1

UNCLASSIFIED

F/G 4/2

NL





XERO COPY RESOLUTION TEST CHART

AD-A186271

REPORT DOCUMENTATION PAGE

1a REPORT SECURITY CLASSIFICATION UNCLASSIFIED		1b RESTRICTIVE MARKINGS	
2a SECURITY CLASSIFICATION AUTHORITY		3 DISTRIBUTION/AVAILABILITY OF REPORT Approved for public release; Distribution is unlimited.	
2b DECLASSIFICATION/DOWNGRADING SCHEDULE		5 MONITORING ORGANIZATION REPORT NUMBER(S)	
4 PERFORMING ORGANIZATION REPORT NUMBER(S)		7a NAME OF MONITORING ORGANIZATION Naval Postgraduate School	
6a NAME OF PERFORMING ORGANIZATION Naval Postgraduate School	6b OFFICE SYMBOL (if applicable) 68	7b ADDRESS (City, State, and ZIP Code) Monterey, California 93943-5000	
6c ADDRESS (City, State, and ZIP Code) Monterey, California 93943-5000		9 PROCUREMENT INSTRUMENT IDENTIFICATION NUMBER	
8a NAME OF FUNDING/SPONSORING ORGANIZATION	8b OFFICE SYMBOL (if applicable)	10 SOURCE OF FUNDING NUMBERS	
8c ADDRESS (City, State and ZIP Code)		PROGRAM ELEMENT NO	PROJECT NO
		TASK NO	WORK UNIT ACCESSION NO
11 TITLE (include Security Classification) An Investigation Of Offshore Circulation Using Satellite Data and Feature Tracking Techniques			
12 PERSONAL AUTHOR(S) Lennon, Gary R.			
13a TYPE OF REPORT Master's Thesis	13b TIME COVERED FROM _____ TO _____	14 DATE OF REPORT (Year, Month, Day) 1987 September	15 PAGE COUNT 41
16 SUPPLEMENTARY NOTATION			
17 COSATI CODES		18 SUBJECT TERMS (Continue on reverse if necessary and identify by block number)	
FIELD	GROUP	SUB-GROUP	
		Offshore Circulation	
		Feature Tracking, Satellite Data Interpretation	
19 ABSTRACT (Continue on reverse if necessary and identify by block number) Satellite-derived sea surface motion vectors are obtained for an area 100 to 300 kilometers from the central California coast south of Point Arena. These vectors are compared with hydrographic data acquired during the OPTOMA 21 cruise. Three AVHRR images, with 24 hour spacing between images, are used to create two sets of sea surface flow vectors. The vectors obtained show only limited agreement with geostrophic velocities computed relative to 750 meters. There is good agreement when the geostrophic flow is strong and persistent submesoscale features are advected by the flow. Unfortunately this technique is only able to identify some of the strong flows and its utility for identifying weak (< 10 cm/sec) flows is questionable. There are numerous eddies and perturbations in the surface flow in this area that cannot be resolved by this technique when the images are 24 hours apart. Cloud contamination in the second image emphasizes the dependence of this technique on an unobstructed view of the ocean. Nevertheless, when used with an understanding of its limitations, the feature tracking technique can be a useful method of interpreting satellite oceanographic data.			
20 DISTRIBUTION/AVAILABILITY OF ABSTRACT <input checked="" type="checkbox"/> UNCLASSIFIED/UNLIMITED <input type="checkbox"/> SAME AS RPT <input type="checkbox"/> DTIC USERS		21 ABSTRACT SECURITY CLASSIFICATION UNCLASSIFIED	
22a NAME OF RESPONSIBLE INDIVIDUAL D. C. Smith IV		22b TELEPHONE (include Area Code) (408) 646-3350	22c OFFICE SYMBOL 68Si

Approved for public release; distribution is unlimited.

An Investigation Of Offshore Circulation
Using Satellite Data and Feature Tracking Techniques

by

Gary R. Lennon
Lieutenant Commander, United States Navy
B.S., University of Washington, 1975

Submitted in partial fulfillment of the
requirements for the degree of

MASTER OF SCIENCE IN METEOROLOGY AND OCEANOGRAPHY

from the

NAVAL POSTGRADUATE SCHOOL
September 1987

Author:

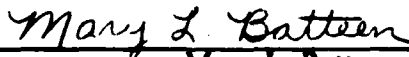


Gary R. Lennon

Approved by:



David C. Smith IV, Co-Advisor



Mary L. Batteen, Co-Advisor

Mary L. Batteen, Co-Advisor



Curtis M. Collins, Chairman,
Department of Oceanography

Curtis M. Collins, Chairman,
Department of Oceanography



Gordon E. Schacher,
Dean of Science and Engineering

Gordon E. Schacher,
Dean of Science and Engineering

ABSTRACT

Satellite-derived sea surface motion vectors are obtained for an area 100 to 300 kilometers from the central California coast south of Point Arena. These vectors are compared with hydrographic data acquired during the OPTOMA 21 cruise. Three AVHRR images, with 24 hour spacing between images, are used to create two sets of sea surface flow vectors. The vectors obtained show only limited agreement with geostrophic velocities computed relative to 750 meters. There is good agreement when the geostrophic flow is strong and persistent submesoscale features are advected by the flow. Unfortunately this technique is only able to identify some of the strong flows and its utility for identifying weak (< 10 cm/sec) flows is questionable. There are numerous eddies and perturbations in the surface flow in this area that cannot be resolved by this technique when the images are 24 hours apart. Cloud contamination in the second image emphasizes the dependence of this technique on an unobstructed view of the ocean. Nevertheless, when used with an understanding of its limitations, the feature tracking technique can be a useful method of interpreting satellite oceanographic data.

Accession For	
NTIS GRA&I	<input checked="" type="checkbox"/>
DTIC TAB	<input type="checkbox"/>
Unannounced	<input type="checkbox"/>
Justification	
By _____	
Distribution/	
Availability Codes	
Dist	Avail and/or Special
A-1	



TABLE OF CONTENTS

I.	INTRODUCTION	7
II.	BACKGROUND	8
	A. PHYSICAL OCEANOGRAPHY OF THE STUDY AREA	8
	B. PREVIOUS SATELLITE DATA STUDIES	9
III.	TECHNIQUE & DESCRIPTION OF THE DATA	12
	A. FEATURE TRACKING	12
	1. Description	12
	B. THE SATELLITE IMAGES	12
	1. Description	12
	2. Error	14
	C. OCEANTRAK	14
	1. Description	14
	2. Error	18
	D. OPTOMA 21	18
	1. Survey Area and Data	18
	2. Error	23
	E. ERROR SUMMARY	23
IV.	RESULTS	26
	A. FEATURE TRACKING VECTORS	26
	B. COMPARISON	31
V.	CONCLUSIONS AND RECOMMENDATIONS	34
	A. CONCLUSIONS	34
	B. RECOMMENDATIONS	35
	LIST OF REFERENCES	37
	INITIAL DISTRIBUTION LIST	38

LIST OF TABLES

1. CTD INSTRUMENT ACCURACIES 23
2. SUMMARY OF MAXIMUM ERRORS 25

LIST OF FIGURES

2.1	Seasonal Variations in the CCS (Ikeda and Emery, 1984)	9
3.1	Channel Four Infrared JULY 14, 1986	15
3.2	Channel Four Infrared JULY 15, 1986	16
3.3	Channel Four Infrared JULY 16, 1986	17
3.4	OPTOMA 21 Station Locations By Date (July)	20
3.5	Buoy Winds 1-23 July, 1986	21
3.6	OPTOMA 21 CTD Station Numbers	22
3.7	Geostrophic Velocities and Dynamic Height Anomalies	24
4.1	Set I Vectors Over July 14 Image	27
4.2	Set I Vectors Over July 15 Image	28
4.3	Set II Vectors Over July 15 Image	29
4.4	Set II Vectors Over July 16 Image	30
4.5	Geostrophic Velocities With Major Features On July 14	32

I. INTRODUCTION

Satellites in service today are providing an important source of oceanographic data. This data covers large areas of the oceans where we have no other source of information. As the library of accumulated information continues to grow, our ability to use it to better understand the oceans becomes directly dependent on our ability to interpret it correctly. The purpose of this study is to investigate one method of interpreting this satellite data.

Oceanographic ships can provide good horizontal and vertical sampling of the ocean in the immediate vicinity of the vessel. However their ability to collect synoptic data over large areas is limited by their relatively slow speeds. The daily operating costs of research vessels is also a limiting factor on how many ships can remain at sea collecting data. While satellite data is currently limited to the surface of the oceans, satellites provide repeat sampling over large areas allowing time series data not available from ships to be obtained.

This study creates sea surface motion vectors using a feature tracking technique applied to three consecutive satellite images of the eastern Pacific Ocean offshore of central California. It is shown that the estimated maximum objective error of the vectors obtained in this study is 3.2 cm/sec. The images are from the AVHRR (Advanced Very High Resolution Radiometer) onboard the NOAA 9 polar orbiting satellite and are separated by 24 hours. These vectors are compared with *in situ* hydrographic data collected during the OPTOMA 21 (Ocean Prediction Through Observation Modelling and Analysis) cruise in July, 1986.

Background information on the general physical oceanographic conditions of the study area and other studies of satellite derived motion are presented in Chapter II. Details of the feature tracking technique and a description of the data are presented in Chapter III. Chapter IV includes the results of the feature tracking and the comparison with the hydrographic data. Conclusions and recommendations are presented in Chapter V.

II. BACKGROUND

A. PHYSICAL OCEANOGRAPHY OF THE STUDY AREA

The area chosen for this study is 100 to 300 kilometers offshore of the central California coast, south of Point Arena. This study area was chosen primarily for two reasons. First, good satellite images with a relatively clear view of the ocean were available for an area where an extensive hydrographic survey had been conducted. Second, there were two large (> 200 km) meanders or features extending offshore from the coast and many small scale variations and perturbations visible in the images which could provide a wide variety of conditions for testing the feature tracking technique. In addition, other studies of the oceanography along this coast provided an excellent background for understanding the overall circulation and the numerous eddies, jets, and other perturbations in the flow field that have been observed.

The California Current is the dominant climatological oceanographic feature at or near the surface of the ocean in this area and is considered to be a part of the California Current System (CCS). The CCS, as described by Hickey (1979), consists of four currents. The California Current is an equatorward flow at the surface that extends offshore in excess of 1000 kilometers in some locations and has as many as three axes of maximum flow. The California Undercurrent is a subsurface poleward flow over the continental slope. The Davidson Current is a poleward surface flow north of Point Conception, occurring during fall and winter. The fourth, the Southern California Countercurrent, is a poleward flow that occurs south of Point Conception and inshore of the channel islands. The flows described in this research are limited to the California Current.

While the California current is generally considered to be a broad, slow moving, eastern boundary current, studies over the last decade have shown that there are many synoptic-mesoscale variations in the current. In addition to seasonal variations described by Ikeda and Emery (1984), that are shown in Figure 2.1, strong filaments (jets) and synoptic-mesoscale eddies have been identified and studied in the California Current

The dominant meteorological feature in this area in the summer is a high pressure area that forms over the eastern Pacific Ocean. The resulting winds are

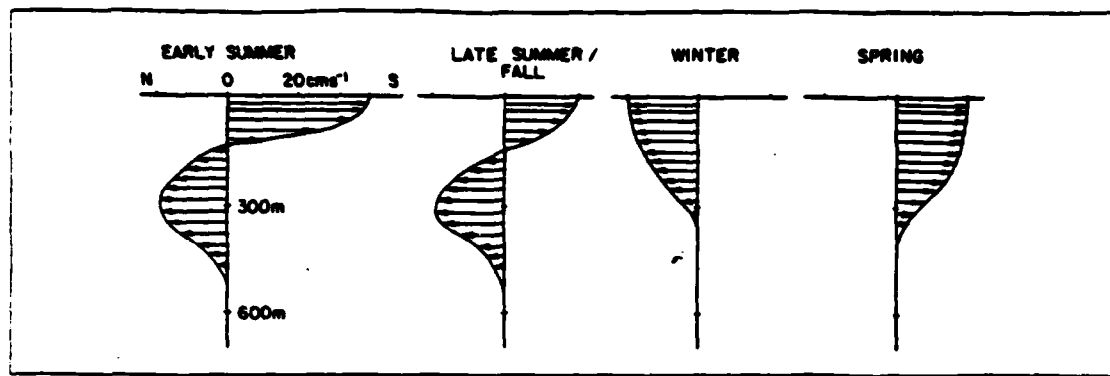


Figure 2.1 Seasonal Variations in the CCS (Ikeda and Emery, 1984).

typically north-northwesterly (alongshore) and are the dominant forcing mechanism for both a southerly flowing coastal jet which is part of the California Current, and Ekman transport offshore. As a result of this transport, strong coastal upwelling is common along the California coast in the summer as seen by the cold sea surface temperatures (SST) near shore.

In addition to this Ekman transport, cold water is transported offshore in strong jets or filaments. These large filaments and jets occur frequently in the summer and fall along the California coast. They may extend several hundred kilometers offshore and are connected to the coastal upwelling region (Flament (1985)). Ikeda and Emery (1984) showed in a modeling study that mesoscale features of this type near Vancouver Island were excited by interactions between the mean current and coastal topography and that they grew due to the baroclinic instability of the vertical shear between the surface current and the undercurrent. When they applied their model to the ocean along the California coast they were able to show the same general results, i.e., their model generated filaments which produced wavelengths similar to those observed along with a cascade of energy to longer wavelengths. In addition to these large filaments, satellite images and ship data have revealed numerous eddies, meanders, and perturbations in the general flow revealing that while the mean flow is relatively slow to the south the mesoscale flow can be quite complex.

B. PREVIOUS SATELLITE DATA STUDIES

Satellite data has been used in several studies relating it directly or indirectly to sea surface motion. After comparing numerous satellite images with *in situ* data Bernstein *et al.* (1977) and Kelly (1983) concluded that sea surface temperature

patterns are representative of surface mesoscale motions. Ikeda and Emery (1984) used infrared satellite images to identify meander patterns in sea surface temperature, i.e., large cold tongues extending offshore, and were able to model their evolution as described earlier. Rienecker *et al.* (1985) used satellite infrared data to follow the motion of a cool anomaly and used this to enhance the analysis of available hydrographic data. Kelly (1985) analyzed sea surface temperature patterns from infrared satellite images and compared them with *in situ* data to investigate the relationship between sea surface temperature patterns and winds, topography, and adjusted sea level. Her analysis suggested that an irregular coastline, and associated effects of coastal mountain winds, generated irregular upwelling patterns and that the cold filaments were anchored to coastal topography. Flament *et al.* (1985) studied an upwelling filament south of Point Arena using hydrographic data and consecutive satellite images. They found that the evolution of small eddies can be followed in consecutive satellite images separated by 12 hours and that the Doppler Acoustic Log (DAL) velocities were approximately 1.5 times faster than the satellite derived vectors.

Vastano and Reid (1985) used a feature tracking technique to estimate the sea surface motion in the vicinity of the Oyashio Front in the northwestern Pacific Ocean. Using an interactive program applied to images 12 to 24 hours apart they tracked submesoscale features that had a temperature gradient of at least four degrees. They showed that advective processes had a higher velocity than Rossby or internal gravity waves. An assumption they used was that vertical motion and heat exchange with the atmosphere were very small compared with horizontal advection of heat during the period of the study. They used the vectors they derived to generate streamfunctions that showed good agreement with the estimated sea surface topography in their study area.

To more objectively measure the variations in the currents studied, Emery *et al.* (1986) developed a feature tracking program that was much less dependent on the operator. The program required images to be converted to SST gradient fields which were analyzed using a maximum cross correlation (MCC) technique. Motion was determined by computing the MCC between a 22 X 22 pixel template window from the first image and a 32 X 32 pixel target window in the second image. While the MCC is computed without operator interaction, the correlation length scales and the pixel windows to be compared are chosen by the operator. In addition the operator must identify clouds and land in the images and ensure these are not in the windows being

compared as both produce inaccurate results. The vectors derived with this technique were generally coherent and showed excellent agreement with shallow drogued drifters. It was observed that this method did not detect rotational or deformational changes which can be accounted for in the interactive feature tracking technique.

O'Hara (1987) compared surface velocity vectors derived with the feature tracking technique with velocity data acquired in a nearshore region of the CCS during the CODE experiment in 1981. Using images twelve hours apart, he found that features became harder to track as he moved closer to the coast. The DAL vectors from a depth of 20 meters were approximately 1.5 time faster than the derived vectors when they were co-located, similar to observations by Flament *et al.* (1985).

III. TECHNIQUE & DESCRIPTION OF THE DATA

A. FEATURE TRACKING

1. Description

Feature tracking is a technique developed to estimate motion in a fluid by tracking identifiable submesoscale features which are advected in the fluid. In this study feature tracking is applied to the ocean surface by identifying and tracking features visible in sequential infrared satellite images. Specifically, a feature is identified in the first image, then the same feature is located in the second image. The distance the feature has moved is measured and from this, and the time interval between the images, a velocity can be computed. The only detectable ocean parameter in an infrared satellite image is sea surface temperature (SST), therefore the features that can be identified and tracked are those occurring where there is a marked change in SST. This technique assumes that the features being tracked are advected by the motion of the water. The vectors derived will accurately represent the sea surface motion only in areas where this assumption is valid. In addition to advection of features, changes in feature location can be caused by waves, by local heating or cooling, and by the formation or dissipation of a feature in the time between images. As a result, feature tracking is a very subjective technique.

In this study two sets of sea surface flow vectors were derived from three sequential infrared satellite images. Set I was derived from comparisons of the images taken on 14 and 15 July. Set II was derived by comparing the images taken on 15 and 16 July. From geostrophy, the flow is expected to be along temperature gradients. The features tracked were submesoscale variations in the temperature gradient assumed to move along it. In all of the images, the most distinct features were identified in areas of strong temperature gradients. The vectors were created with the Oceantrak program described below.

B. THE SATELLITE IMAGES

1. Description

Three concurrent satellite images were obtained on three consecutive days from the five channel AVHRR carried onboard the polar orbiting NOAA 9 satellite. The three concurrent images were the visible image from channel one (0.55 - 0.68 μm),

and the infrared images from channels four (10.3 - 11.3 μm), and five (11.5 -12.5 μm). The images were from the daytime passes on 14, 15, and 16 July, 1986, taken about 2300 GMT (1600 Pacific Daylight Time) each day. All images were received and initially processed at the Satellite Oceanography Facility of the Scripps Oceanographic Institute. The images were chosen to coincide with the area being surveyed by the R/V POINT SUR as part of OPTOMA 21. These were the three clearest consecutive images obtained during the cruise.

The enhanced channel four infrared images for July 14, 15, and 16 are shown in Figures 3.1, 3.2, and 3.3 respectively. On July 14 there was an extensive layer of low stratus clouds along the coast south of 38.5 N. There was some coastal cloudiness north of this that did not extend more than fifteen kilometers offshore at its widest point. This did not effect the offshore feature tracking but it did blur some of the points along the coast that could be used as landmarks. There was a large band of broken cloudiness extending in from the western edge of the image, however it masks only the southwestern most OPTOMA stations. On July 15th there was coastal cloudiness only along the southeast edge of the image and in the vicinity of Cape Mendocino. The offshore cloudiness extended from the western edge of the image east to approximately 125.5 W. This masked part of the most prominent features in the image and, as a result, reduced the number of features that could be tracked. July 16th was almost completely clear in the area surveyed by the POINT SUR with only some very thin clouds on the extreme northern and southern edges.

The raw data were calibrated in aperture brightness temperature and resampled on an equi-rectangular map grid centered on the latitude of Pt. Reyes (38 North). The error introduced by using this projection is discussed below. The resulting images were 512 X 512 pixel images that include the California coast and extend approximately four hundred kilometers offshore. Digital data files of all nine images were provided to the Naval Postgraduate School on magnetic tape. Photographs of the channel four infrared images with positional grid points indicating the intersection of whole degrees of latitude and longitude overlaid on the images were also provided.

The images were processed and manipulated at NPS using a Comtal Vision One image processor (COMTAL) in conjunction with a Digital Equipment Corporation VAX 11/780 computer. The infrared images were enhanced using a program that converts the land to black (pixel value = 0) and the clouds to white (pixel value = 255), and makes the gray shades from the ocean more distinct. This

enhancement of the images made the identification of features more precise. Concurrent visible and enhanced infrared images were examined and compared to identify cloud coverage that would mask or modify the apparent SST.

The clouds that can be identified can be converted to a uniform gray shade that can be avoided when choosing features to track. In this study clouds were converted to white (pixel value = 255). While they may mask features, they should not cause errors in the results. Clouds that are smaller than the 1.1 kilometer resolution of the images, however, can introduce errors by changing the apparent sea surface temperature in the pixel they are included in, thereby possibly modifying the appearance of a feature.

Comparison of concurrent channel four and channel five infrared images was done to determine which channel would be used for the feature tracking. When displayed on the COMTAL there was little difference between the two channels in definition of features. The channel four infrared images were selected for the feature tracking because the features in the survey area appeared to be slightly better defined on the COMTAL. A correction for atmospheric moisture was not made in view of observations by Emery *et al.* (1986), that the spatial scales of atmospheric moisture are much larger than the sea surface temperature features being tracked and because temperature gradients, rather than absolute temperature, were expected to be used to define the features.

2. Error

The satellite images were processed and registered to an equi-rectangular latitude/longitude grid when they were received. Slight variations in the received images and in the processing can result in two images of the same area not being exactly the same. Coregistration errors can cause errors in the computed velocities if they are not identified and corrected in the feature tracking process. Actual coregistration errors are listed below.

C. OCEANTRAK

1. Description

Oceantrak is an interactive Fortran program, tailored for use with the COMTAL, that allows the user to compare two images and create vectors representative of the movement of individual features between images. It is a modified version of a program originally written to compute cloud drift winds. The program works by allowing the user to alternate between two images on the COMTAL and to

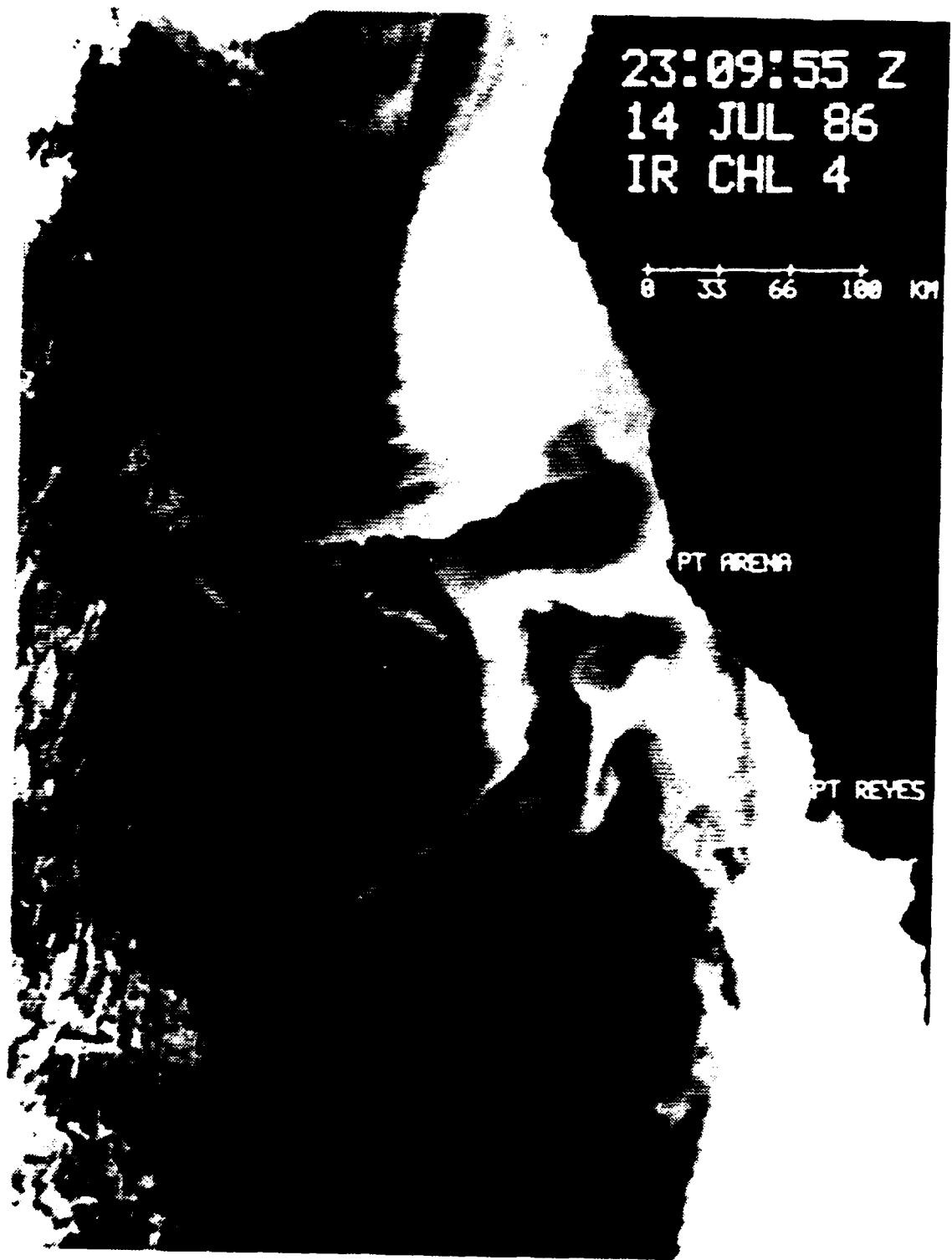


Figure 3.1 Channel Four Infrared JULY 14, 1986.

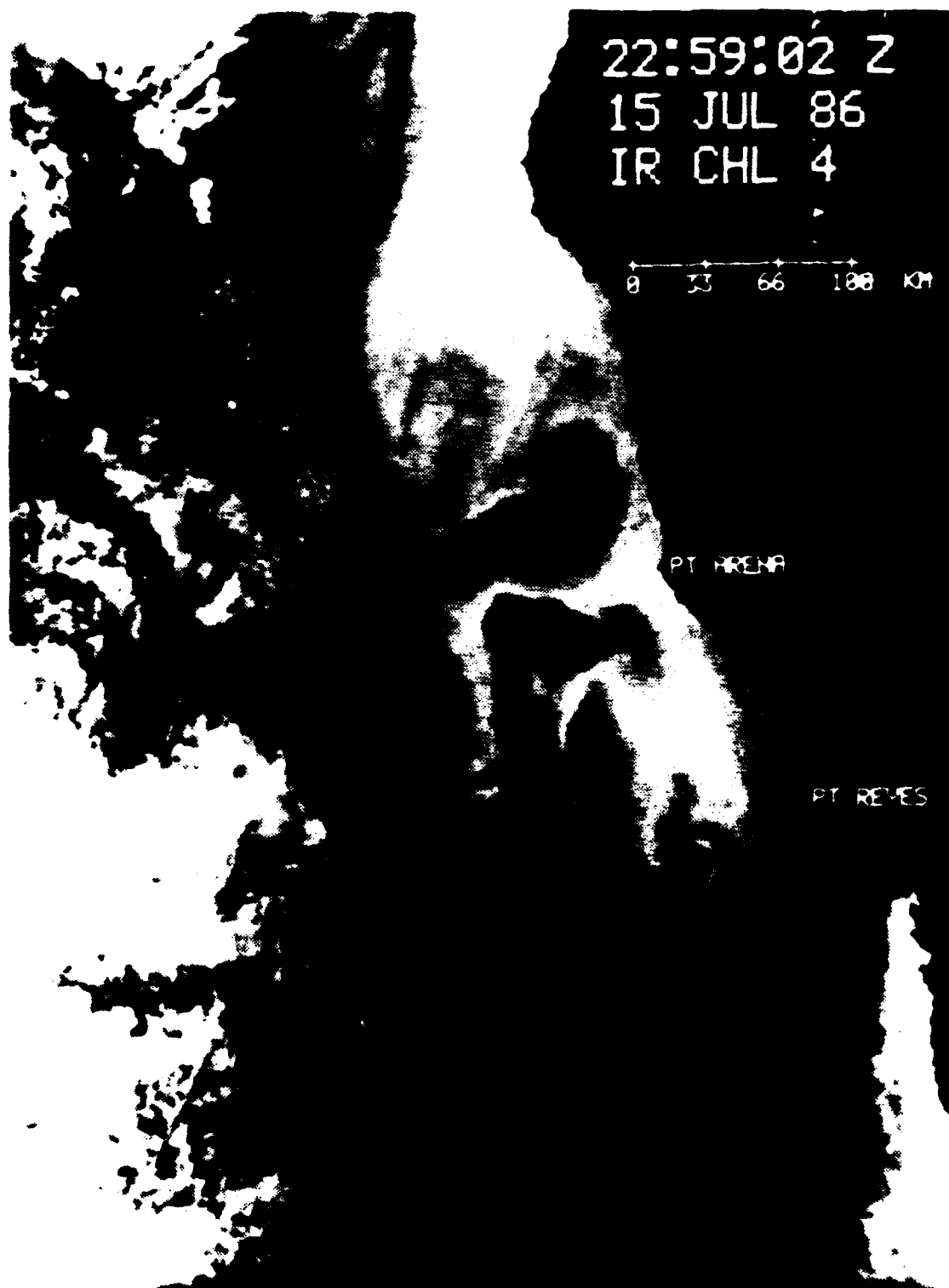


Figure 3.2 Channel Four Infrared JULY 15, 1986.



Figure 3.3 Channel Clear Infrared - 11 JUL 1986

specify the location of a feature with the cursor. When the user is satisfied that the feature is accurately marked on both images, the program can create a vector representing straight line motion between the two points specified by the cursors. The user inputs the time each image was taken and the program uses these and the 1.1 kilometer pixel scale of these images to compute the velocity in cm/sec that would be required for a feature to move a distance of one pixel. This value is expressed as cm per pixel per sec (cm/p/sec). The number of pixels the feature has moved is calculated from the specified cursor positions. From these two values the velocity is computed. Features tracked in this study were submesoscale bends, kinks, apparent crests or troughs, and other small scale, but well defined, variations.

2. Error

The Oceantrak program can both introduce errors and be used to identify errors. Oceantrak uses a single time for each image when it computes velocities. The time assigned to each image used in this study was the "crossing" time for Pt. Reyes. As the images were actually taken over a period of approximately 90 seconds, a small error can occur. The time between images was approximately 85,800 seconds resulting in an insignificant maximum error of 1×10^{-3} cm/p.sec (~ 0.1 percent). Oceantrak can be used to quantify the error due to imperfect coregistration of the images by identifying fixed landmarks in both images and using Oceantrak to compute the apparent motion of these fixed points. Identification of landmarks along the coast in these images was hampered by the coastal cloudiness and haze. In set I, one landmark was stationary, and the other two showed unequal motion. In set II, the three landmarks all had unequal motion. This indicates that the coregistration error is probably due to a slight rotation of the image, poor resolution due to coastal cloudiness or haze that could not be identified, or a small timing error at the satellite receiving station. The COMTAL can be used to move an entire image by single pixel values in the x or y direction on the screen. Current software available does not provide for rotation of the image in other than 90 degree increments. As a result coregistration errors are added to the error budget summarized below.

D. OPTOMA 21

1. Survey Area and Data

The OPTOMA program was a joint effort between NPS and Harvard University, funded by the Office of Naval Research, to study the California Current System (CCS) with the goal of being able to predict mesoscale motion in the CCS if

given a set of initial conditions. The OPTOMA 21 cruise, from 7 through 20 July, 1986, surveyed the area shown in Figure 3.4. All stations taken are shown with the date (July) they were taken. This particular section of the CCS was selected in order to sample two large (200 km) meanders or jets and the associated smaller scale variations in this area that had been identified on satellite images of the area.

Winds in the study area were generally alongshore, from the north-northwest, at 8 to 10 m sec from the end of June. A stick diagram of buoy winds from 1 through 23 July is shown in Figure 3.5. While the buoy is northeast of the primary features being studied, the winds are representative of those observed in the study area. These winds are typical for this area in July and are very favorable for coastal upwelling.

Hydrographic sampling was conducted at 121 expendable bathythermograph (XBT) stations and at 73 stations using a conductivity, temperature, and depth (CTD) sensor. CTD station numbers are shown in Figure 3.6. The maximum depth sampled in this survey was 750 meters. Of the 194 stations taken, 100 XBT and 47 CTD were taken to this depth. When the data were processed, temperature - salinity relationships were computed using the CTD data. From these a salinity was assigned to each XBT temperature so that as a result the salinity values assigned to the XBT data were an average of the salinities from different parts of the survey area. Because variations in salinity have a significant effect on geostrophy, the XBT data were not used to compute geostrophic velocities.

The level of no motion (LNM) for computing geostrophic velocities was chosen as 750 m because this is the deepest depth to which stations were taken on this survey and all but one of the CTD stations well offshore were taken to this depth. In studying a cool anomaly off northern California, Rienecker *et al.* (1985) concluded that in using 450 meters as the LNM, the computed geostrophic speeds would be a lower bound on the actual geostrophic speeds but that the horizontal structure of the surface flow field was not likely to show a significant change if a deeper LNM was used. From a climatological view, 750 meters should be well below the most active part of the local currents (see Figure 2.1). In view of the accuracies of the feature tracking technique, using a deeper LNM should not significantly change the results even if the data were available.

Objective analysis of the dynamic height field was considered but not used because of the much shorter time scale over which feature tracking is applied. The changes observed in the ocean in the 24 hours between images could not be accurately

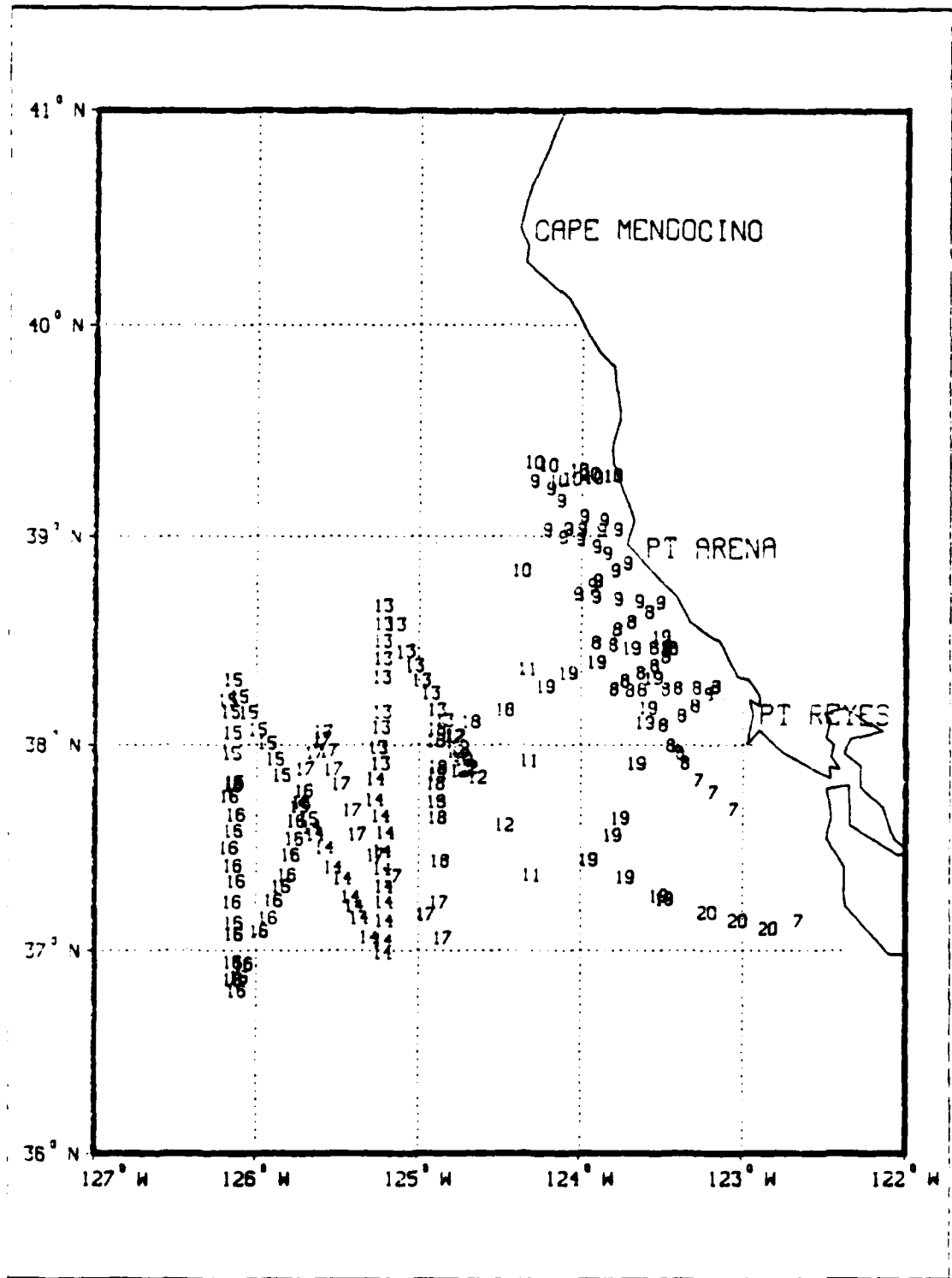


Figure 3.4 OPTOMA 21 Station Locations By Date (July).

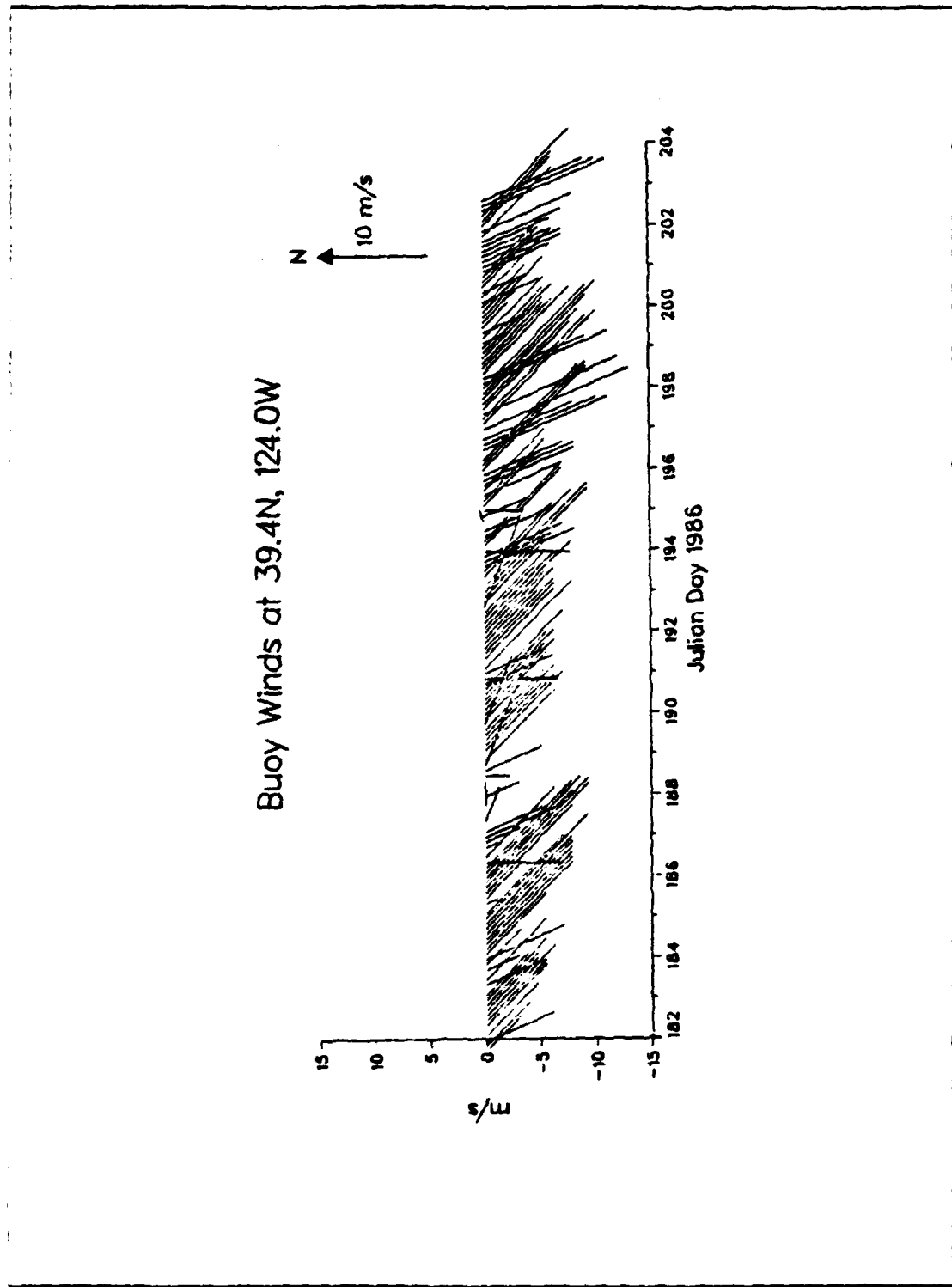


Figure 3.5 Buoy Winds 1-23 July, 1986.

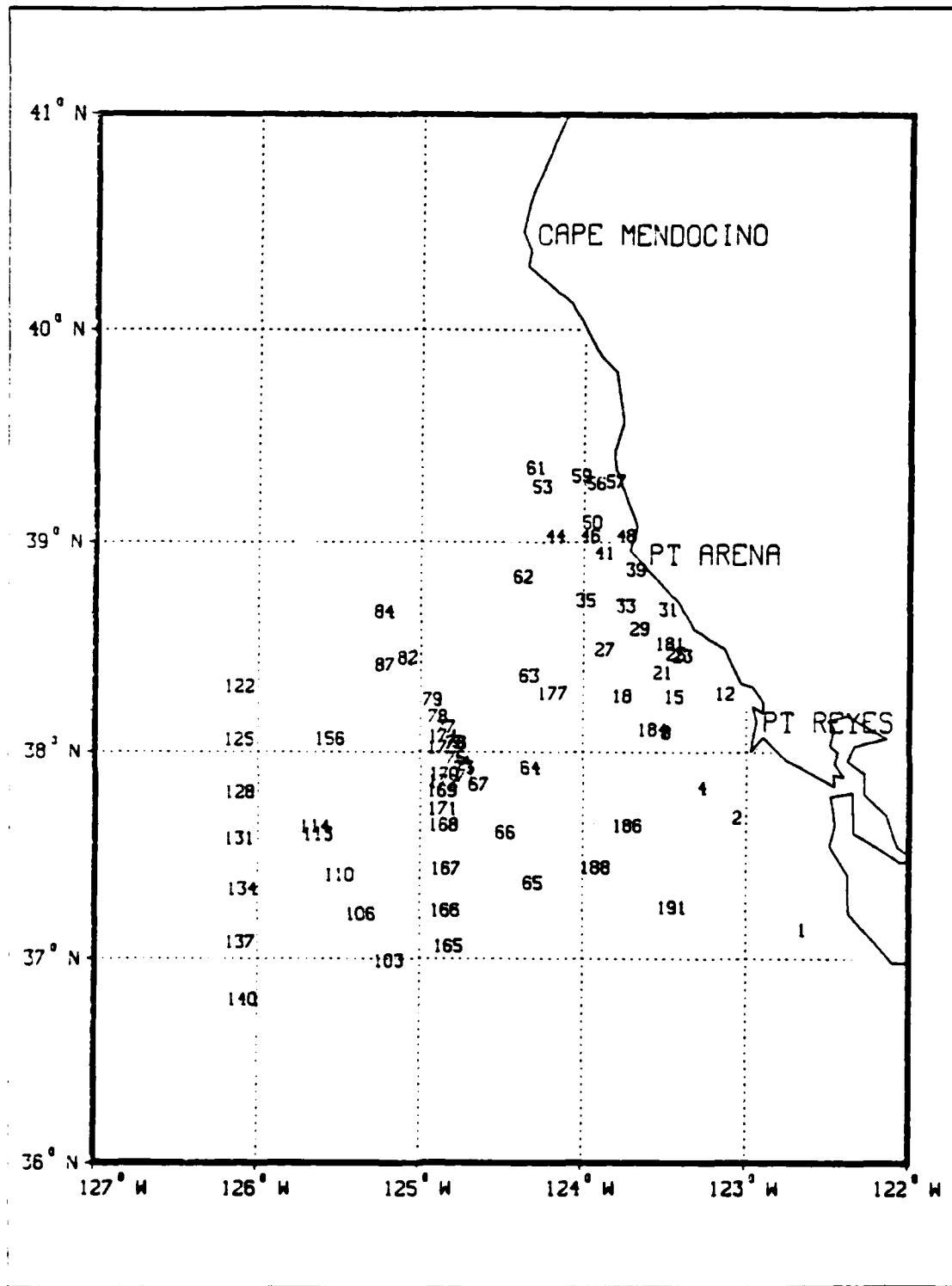


Figure 3.6 OPTOMA 21 CTD Station Numbers.

reflected by objective analysis over eight days due to the temporal averaging inherent in the process.

Geostrophic velocities computed between CTD stations taken 11 through 18 July are shown in Figure 3.7 with dynamic height anomalies computed at these stations. Geostrophic velocities are in cm/sec while dynamic height are in meters. The flow patterns are described below.

2. Error

The maximum error in the geostrophic velocities comes from inaccuracies in the navigation of the ship. The CTD data were collected with a Mark IIIb Neil Brown CTD. Sensor accuracies for this instrument are shown in Table 1. Water samples were taken at each station for calibration of the conductivity meter and the thermistor was calibrated before and after the cruise. In both cases the variations were so small that no corrections were made to the data. The ship's position was fixed using LORAN C with an accuracy of .1 kilometer. With CTD stations 25 to 30 kilometers apart, this

TABLE 1
CTD INSTRUMENT ACCURACIES

Variable	Sensor	Accuracy	Resolution
Pressure	Strain gauge	1.6 dbar	0.025 dbar
Temperature	Thermistor	0.005 C	0.005 C
Conductivity	Electrode cell	0.005 mmho	0.005 mmho

results in a maximum error of approximately 1 percent.

E. ERROR SUMMARY

Imperfect coregistration of the satellite images was the largest source of error in the feature tracking technique. The maximum error from this was 2.9 cm/sec in both sets of vectors. The actual magnitude and direction of this error is dependent on the direction of the derived vector. Since this error is not dependent on the magnitude of the derived vector, the larger vectors will have a smaller percentage error from this cause.

An equi-rectangular grid has an equal distance between latitude lines and between longitude lines. As the longitude lines converge in the poleward direction on the earth, some distortion is created when the raw data are resampled or projected onto this grid. Most of the data are within one degree of the reference latitude (38N) of the image. The change in pixel width (east-west) one degree north or south of the reference latitude is approximately 15.5 meters. This results in a velocity computation error of .018 cm/p sec or ~ 1.4 percent. To exactly navigate the image the crosstrack enlargement of the area encompassed by one pixel (approximately 1.5 kilometers at the outer edge of the sweep) would have to be resolved with spherical geometry. This correction was not applied because the study area is not near the edge of the AVHRR sweepwidth.

A summary of errors is shown in Table 2. These are the maximum errors expected for each error source.

TABLE 2
SUMMARY OF MAXIMUM ERRORS

ERROR SOURCE	NORTH-SOUTH ERROR (cm/sec)	EAST-WEST ERROR (cm/sec)
Equi-rectangular Projection	~ 0	$.018^{.58}$ cm/p/sec
Crossing Time	.0007	~ 0.1
Inaccurate Coregistration		
Set I	1.3	2.6
Set II	1.3	2.6
Geostrophic Velocity	~ 1 percent	

IV. RESULTS

A. FEATURE TRACKING VECTORS

In general the flow field is a complex mix of alongshore and crossshore motion. The satellite images show the strong cross-shelf thermal contrast indicative of alongshore southward flow. In addition, however, the geostrophic flow field shows two regions of strong cross-shelf "filament" motion.

The vectors derived using the feature tracking technique show good agreement with the computed geostrophic velocities at some points and very poor agreement at others. The vectors derived from comparing the images taken on 14 and 15 July (referred to as set I) are shown in Figure 4.1, superimposed over the image taken on July 14 while Figure 4.2 shows them superimposed over the image taken on July 15. Figure 4.3 shows the vectors derived from comparing the images taken on 15 and 16 July (referred to as set II) superimposed over the image taken on July 15 and Figure 4.4 shows set II superimposed over the image taken on July 16. The velocity and distance scales are shown on each plot. The vectors are scaled such that the base of the vector is at the position of the feature on the first day, and the head of the vector is in the proximity of the position of the feature on the second day.

The feature at A in Figure 4.1, along the interface between the colder water to the north and the warmer water to the south appears to be a wave with a westward phase speed of 35.5 cm/sec. This is opposite to the direction expected from temperature dominated geostrophic flow. This wave continues westward in set II with a velocity of 41.9 cm/sec. By July 16, another wave has formed along the eastern part of this interface with three distinct crests. The wave evident at this interface has moved westward in an image taken at 2215 GMT on July 17. This wave form is very similar to one encountered in a study by Ramp (1983) of the interaction of the northern edge of a warm core Gulf Stream ring with the colder, oppositely flowing, coastal water to the north. He concluded that the cause of the wave was a combination of barotropic and baroclinic instabilities.

In the vicinity of B, both sets of vectors show a flow to the northwest over the 48 hours covered by the images. The northern boundary of the warmer water in this area has become a well defined wedge by July 16. This flow is opposite to the direction of

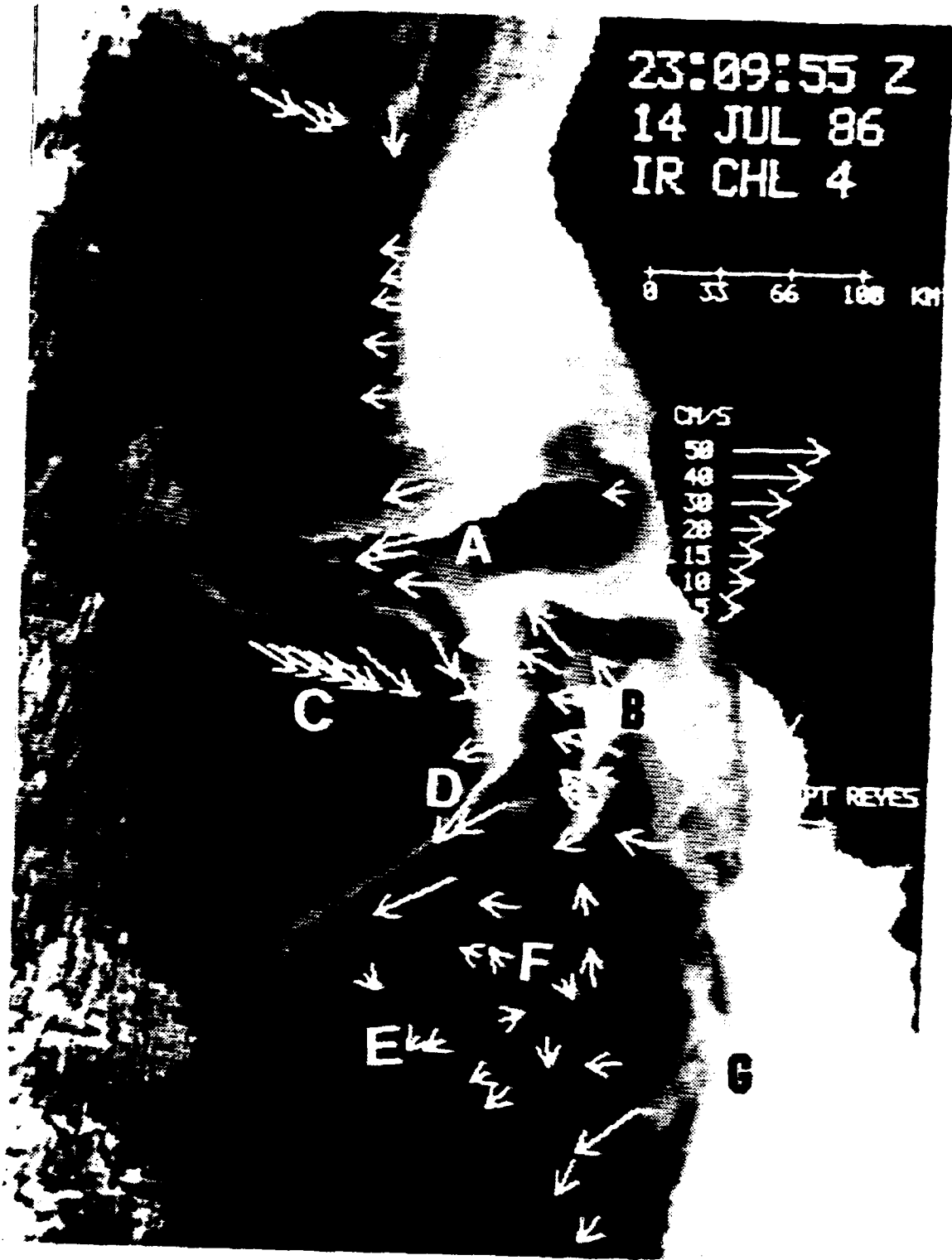


Figure 4.1 Set I Vectors Over July 14 Image.

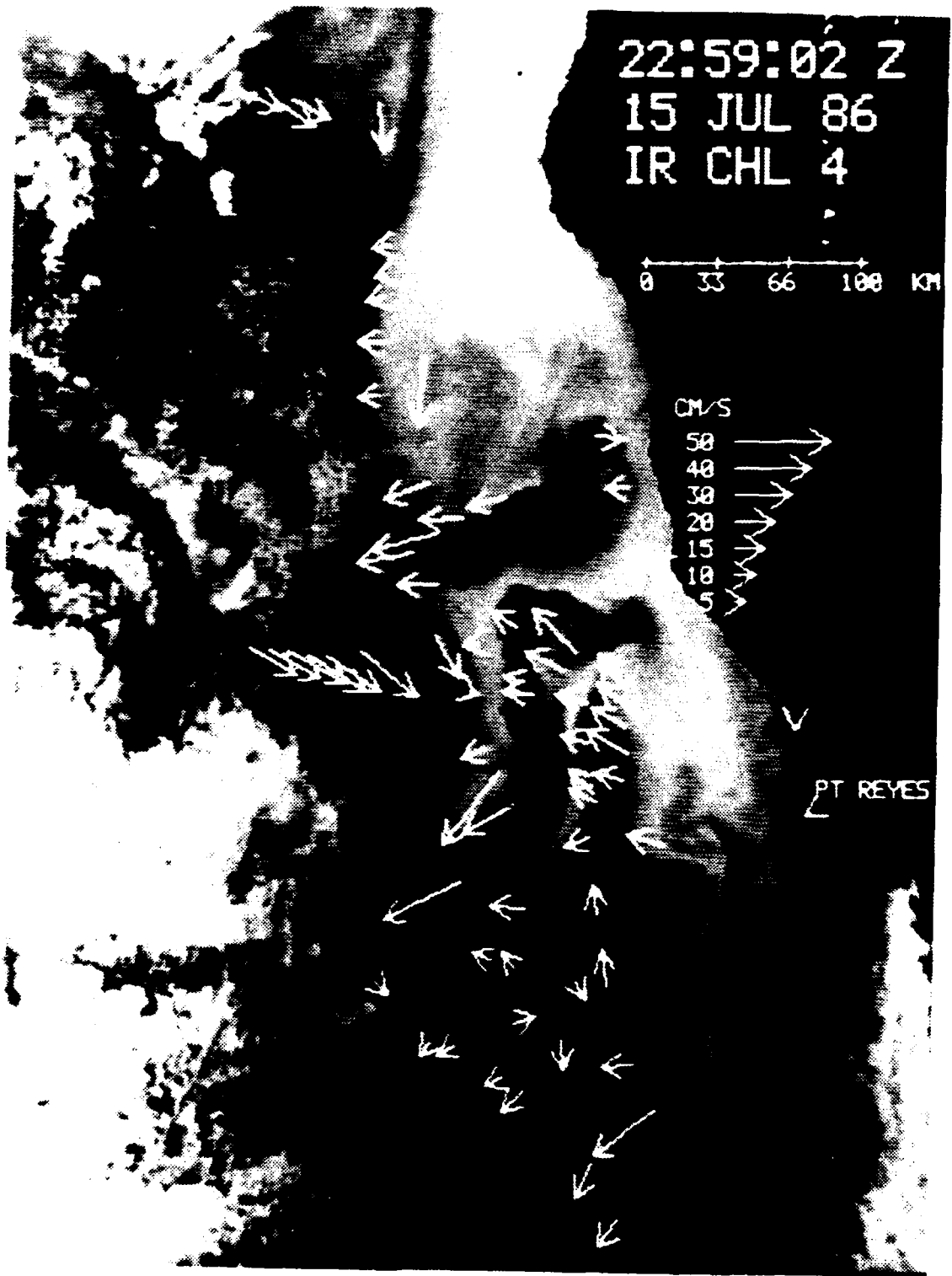


Figure 4.2 Set I Vectors Over July 15 Image.



Figure 4.3 Set II Vectors Over July 15 Image.

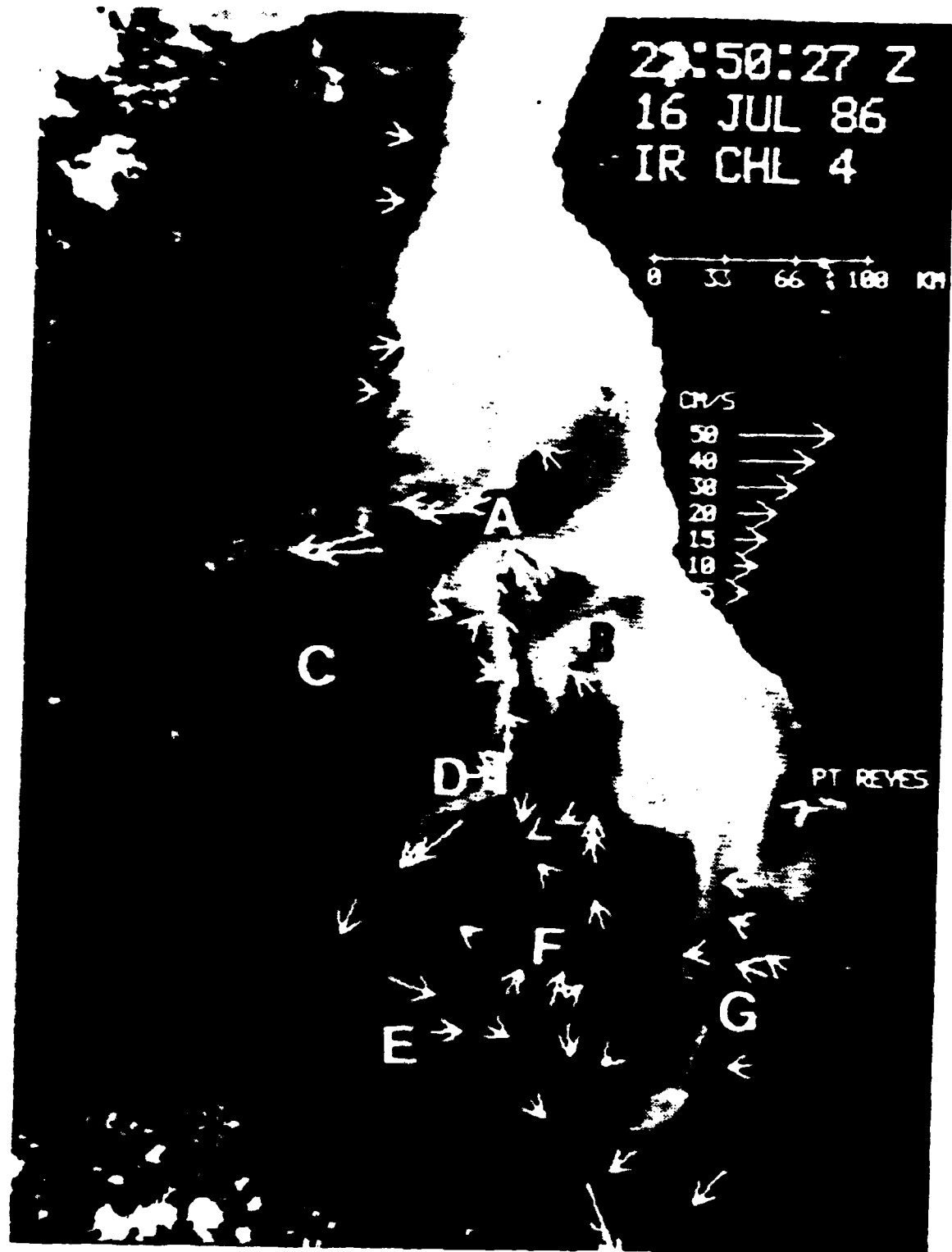


Figure 4.4 Set II Vectors Over July 16 Image.

the wind and the dominant forcing mechanism is not known. The colder water to the east in this area has moved continually offshore in these three images and continues to do so on July 17. By 2215 GMT on July 17 the northern part of the warmer water has curled strongly to the left and continued to push to the northwest.

The vectors at C show a uniform flow in this area, generally in the same direction as to the wind, in set I. This flow is consistent with geostrophic flow where temperature dominates, and appears to be a return flow to the east from the filament of which it is part. There were no trackable features visible on July 16 in this area.

The vectors along the front at D in Figure 4.1 show a strong southwest flow into a cold meander. Unfortunately clouds have masked the western end of this large scale flow on July 15 preventing any derivation of vectors in that area. In set II a southwest flow is also observed in this area however the strength is noticeably weaker than in set I.

The flow at E in set I is weak to the southwest. Only one vector was obtained along the axis of the cold filament in this area. From an inspection of the images, the flow in the vicinity of E appears to be a continuation of the meander at D. However correlation of features between images proved to be very difficult in this area. This may account for some of the variability between sets and the disagreement with geostrophic velocities in this area. In set II, the vectors derived in this area are all generally parallel to the axis of the cold filament and the velocities are generally stronger than those derived in set I.

The flow at F is weak and generally cyclonic in both vector sets. The eastern extent of this weak cyclonic motion is well defined by two southerly vectors in set I. It extends farther to the east in set II and may extend all the way to the offshore flow at G.

B. COMPARISON

Geostrophic velocities used for comparison with the derived vectors were limited to those computed from stations taken on July 11 through July 18. The geostrophic velocities and dynamic height anomalies shown in Figure 3.7 have been overlaid with the most distinctive features visible on July 14, and are shown in Figure 4.5. Set I shows good agreement with the geostrophic velocities in the vicinity of C and D even though the stations were taken as much as 48 hours before the first image in this set. The maximum geostrophic velocity of 41.8 cm.sec at D compares very well with the 46.2 cm.sec velocity derived at that location. The velocities north and south of this

point also compare well. Set I shows very poor agreement with the geostrophic velocities in the area of E. While the derived velocities are approximately 10 cm sec to the southwest, the computed velocities are as high as 57.7 cm sec to the northeast. Just to the north, at F, the velocities are comparable and both support a weak cyclonic flow in this area.

Derived velocities in set II were generally weaker than those in set I. A relatively strong flow at D is in general agreement with the computed velocities, and the flow at E is generally in the direction of the computed velocities but much weaker. The flow north of D is weak and variable, and cannot be correlated with the geostrophic velocities.

The repeatability of this technique was poor in these images. The two sets of vectors were qualitatively similar at A, B, and F. They were not similar at D or E, and were not available at C in set II. There were major differences between the sets at D and E even though the geostrophic velocities in these areas were similar in data taken four days apart.

The temporal separation between the time when the the satellite images were taken and when the hydrographic data was taken has resulted in a temporal discontinuity of 48 hours or more in some of these comparisons. Although this reduced the significance of a direct correlation, approximate correlations should still be valid.

V. CONCLUSIONS AND RECOMMENDATIONS

A. CONCLUSIONS

The ocean surface velocity vectors derived using the feature tracking technique show only partial agreement with the hydrographic data collected during the same general period. The technique correctly identifies some of the strong flows, but not all of them. It does a poor job identifying velocities less than 10 cm sec. In general it underestimates the geostrophic flow velocities. The 24 hour spacing between images results in velocity vectors that are an average of the motion of one particular feature over that time period. The temporal spacing between pairs of CTD stations used to compute geostrophic velocities varied from 1.6 to 5.2 hours. Therefore the two methods are actually measuring two different velocity fields. One is a concurrent set of vectors averaging the motion over 24 hours, while the other is a series of two to five hour averages, measured consecutively. In the consecutive set there is as much as 30 hours between station pairs used to compute the geostrophic velocity vectors. With 24 hours between images, the feature tracking technique cannot resolve small scale surface flow, yet it uses small scale variations to measure velocity. Eddies or perturbations that develop, dissipate, or change significantly in 24 hours cannot be tracked and could be difficult to identify.

Feature tracking is most accurate in areas with very strong temperature gradients. In the offshore region, this is usually the area of strongest flow if the winds are weak, because geostrophic flow will dominate. If there is a prolonged moderate or strong wind, the surface flow can be significantly modified from geostrophy due to direct wind forcing, Ekman pumping offshore, or Ekman transport near the coast. The features in areas of weaker temperature gradients are harder to define accurately in the infrared images. For example the vectors in area D were hard to define in set II even with the set I vectors as a guide. Even though the stronger temperature gradient in this area produced sharper features, the stronger flow and shear provided more forcing to change the features in the time frame between images.

Horizontal waves such as the one near A in Figure 4.1 can be tracked using this technique. This provides a relatively simple method to track waves compared to tracking them from ships, since ships can only track them if they happen to be in the

area where the wave is occurring. These waves, however, are not indicative of geostrophic flow.

Correlation with data from other sources is sensitive to the positional accuracy of the vectors created. When the image of a spherical sea surface is transferred to a flat rectangular grid, some distortion will occur. Even if the image includes a coastline to use as a reference, latitude and longitude lines will still not be straight lines through or parallel to the reference points. An accurate positional grid can be obtained if the initial processing station that receives the raw data can take the navigational information from the satellite and put a positional grid on the image. By marking all intersection points of whole degrees of latitude and longitude features can be more accurately navigated and correlated with other data.

The COMTAL image processor was used to magnify the images by a factor of four which presented a more detailed view of the area. This was found to be useful in determining the best boundary for the features being tracked. When these vectors were compared with vectors derived from the same features without the magnification, half were found to be different.

The very subjective nature of feature identification, and its dependence on the constantly changing small scale variations in the ocean, result in inconsistent reliability, at least for the complex mesoscale field of the CCS. Because the technique may not identify all of the strong flows its utility for the initialization of numerical models is questionable. In general the feature tracking technique is very dependent on the temporal spacing of the images and a clear view of the ocean. Under these conditions the technique can provide an accurate measure of some strong sea surface motions. When used with an understanding of its limitations, the feature tracking technique can be a useful method of interpreting satellite oceanographic data.

B. RECOMMENDATIONS

Feature tracking can be a useful method for interpreting satellite data as long as we remember the original assumptions made with this technique and are aware of its limitations.

Using images with a smaller temporal spacing would provide greater accuracy, assuming the features are not masked by clouds or haze. Using multiple consecutive images would aid in identifying persistent features. Conversion of the image to a gradient scale may better define the features thereby making them easier to track accurately.

Comparison with Doppler Acoustic Log (DAL) data in addition to geostrophic velocities would provide a verification of direction and velocity. This is true if the motion at the level of the DAL data is the same as at the surface. Comparison with other data would be improved if an accurate positional grid is overlaid on or included in the image.

LIST OF REFERENCES

- Bernstein R. L., L. Breaker and R. Whirner, 1977: California Current eddy formation: Ship, air and satellite results. *Science*, **195**, 353-359.
- _____, 1982: Sea surface temperature estimation using the NOAA 6 satellite advanced very high resolution radiometer. *J. Geophys. Res.*, **87**, 9455-9465.
- Emery, W. J., A. C. Thomas, M. J. Collins, W. R. Crawford and D. L. Mackas, 1986: An objective method for computing advective surface velocities from sequential infrared satellite images. *J. Geophys. Res.*, **91**, 12865-12878.
- Flament P., L. Armi and L. Washburn, 1985: The evolving structure of an upwelling filament. *J. Geophys. Res.*, **90**, 11765-11778.
- Ikeda, M., and W. J. Emery, 1984: Satellite observations and modeling in the California current system off Oregon and northern California. *J. Phys. Oceanogr.*, **14**, 1434-1450.
- Kelly, K. A., 1983: Swirls and plumes or application of statistical methods to satellite-derived sea surface temperatures, Ph.D. thesis, *SIO Ref. 83-15, CODE Tech. Rep. 18*, Scripps Inst. Oceanogr., La Jolla, CA, 210 pp.
- _____, 1985: The influence of winds and topography on the sea surface temperature patterns over the northern California slope. *J. Geophys. Res.*, **90**, 11783-11798.
- O'Hara, J. F., 1987: A Comparison of Satellite-Derived Ocean Velocities With Observations in the California Region, Masters Thesis. Naval Postgraduate School, Monterey, CA, 40 pp.
- Ramp, S. R., R. C. Beardsley and R. Legeckis, 1983: An Observation of Frontal Wave Development on a Shelf-Slope/Warm Core Ring Front Near the Shelf Break South of New England. *J. Phys. Oceanogr.*, **13**, 907-912.
- Rienecker, M. M., C. N. K. Mooers, D. E. Hagan, and A. R. Robinson, 1985: A cool anomaly off Northern California: an investigation using IR imagery and in situ data. *J. Geophys. Res.*, **90**, 4807-4818.
- Vastano, A. C., and R. O. Reid, 1985: Sea surface topography estimation with infrared satellite imagery. *J. Atmos. Ocean. Tech.*, **2**, 393-400.

INITIAL DISTRIBUTION LIST

		No. Copies
1.	Defense Technical Information Center Cameron Station Alexandria, VA 22304-6145	2
2.	Library, Code 0142 Naval Postgraduate School Monterey, CA 93943-5002	2
3.	Chairman (Code 68Co) Department of Oceanography Naval Postgraduate School Monterey, CA 93943-5000	1
4.	Chairman (Code 63Rd) Department of Meteorology Naval Postgraduate School Monterey, CA 93943-5000	1
5.	Professor D. C. Smith IV (Code 68Si) Department of Oceanography Naval Postgraduate School Monterey, CA 93943-5000	2
6.	Professor M. L. Batteen (Code 68Bv) Department of Oceanography Naval Postgraduate School Monterey, CA 93943-5000	2
7.	Professor Robert L. Haney (Code 63Hy) Department of Meteorology Naval Postgraduate School Monterey, CA 93943-5000	1
8.	LCDR Gary R. Lennon Deck Department USS Dwight D. Eisenhower (CVN-69) FPO New York, NY 09532-2830	2
9.	Director Naval Oceanography Division Naval Observatory 34th and Massachusetts Avenue NW Washington, DC 20390	1

- | | | |
|-----|---|---|
| 10. | Commander
Naval Oceanography Command
NSTL Station
Bay St. Louis, MS 39522 | 1 |
| 11. | Commanding Officer
Naval Oceanographic Office
NSTL Station
Bay St. Louis, MS 39522 | 1 |
| 12. | Commanding Officer
Fleet Numerical Oceanography Center
Monterey, CA 93943-5005 | 1 |
| 13. | Commanding Officer
Naval Ocean Research and Development Activity
NSTL Station
Bay St. Louis, MS 39522 | 1 |
| 14. | Commanding Officer
Naval Environmental Prediction Research Facility
Monterey, CA 93943-5006 | 1 |
| 15. | Chairman, Oceanography Department
U.S. Naval Academy
Annapolis, MD 21402 | 1 |
| 16. | Chief of Naval Research
800 N. Quincy Street
Arlington, VA 22217 | 1 |
| 17. | Office of Naval Research (Code 420)
Naval Ocean Research and Development Activity
800 N. Quincy Street
Arlington, VA 22217 | 1 |
| 18. | Scientific Liaison Office
Office of Naval Research
Scripps Institution of Oceanography
La Jolla, CA 92037 | 1 |
| 19. | LT John F. O'Hara
257 Beaver Dam Rd.
Scituate, MA 02066 | 1 |
| 20. | M. L. Ciandro
Scripps Institution of Oceanography
Scripps Satellite Oceanography Facility
Code A-014
La Jolla, CA 92093 | 1 |

21. T. Stanton (Code 68St) 1
Department of Oceanography
Naval Postgraduate School
Monterey, CA 93943-5000
22. LCDR Chung-ming Fang 1
Chinese Naval Hydrographic and Oceanographic Office
Tsoying, Kaohsiung
Taiwan 813
Republic of China
23. J. Nystuen (Code 68Ny) 1
Department of Oceanography
Naval Postgraduate School
Monterey, CA 93943-5000
24. Dr. Christopher N. K. Mooers 1
The Institute for Naval Oceanography
NSTL, MS 39529-5005

END

DATE

FILMED

DEC.

1987